



# Climate response to off-equatorial stratospheric sulfur injections in three Earth System Models - Part 2: stratospheric and free-tropospheric response

5 Ewa M. Bednarz<sup>1</sup>, Daniele Visionsi<sup>1</sup>, Ben Kravitz<sup>2,3</sup>, Andy Jones<sup>4</sup>, James M. Haywood<sup>4,5</sup>, Jadwiga Richter<sup>6</sup>, Douglas G. MacMartin<sup>1</sup>, Peter Braesicke<sup>7</sup>

1. Sibley School of Mechanical and Aerospace Engineering, Cornell University, Ithaca, NY, USA

2. Department of Earth and Atmospheric Sciences, Indiana University, Bloomington, IN, USA

10 3. Atmospheric Sciences and Global Change Division, Pacific Northwest National Laboratory, Richland, WA, USA

4. Met Office Hadley Centre, Exeter, UK

5. College of Engineering, Maths and Physical Science, University of Exeter, Exeter, UK

6. National Centre for Atmospheric Research, Boulder, CO, USA

7. IMK-ASF, Karlsruhe Institute of Technology, Eggenstein-Leopoldshafen, Germany

15

*Correspondence to:* Ewa M. Bednarz (ewa.bednarz@cornell.edu)

## Abstract.

The paper constitutes part 2 of a study performing a first systematic inter-model comparison of the atmospheric responses to stratospheric sulfate aerosol injections (SAI) at various latitudes as simulated by three state-of-the-art Earth System Models -  
20 CESM2(WACCM6), UKESM1.0, and GISS-E2.1-G. We use a set of five sensitivity experiments with constant annual injections of SO<sub>2</sub> in the lower stratosphere at either 30° S, 15° S, 0°, 15° N or 30° N. We identify the similarities and differences in the simulated responses amongst the models as well as demonstrate the role of biases in the climatological circulation and specific aspects of the model microphysics and chemistry in driving the inter-model differences

25 Building on part 1 (Visioni et al., 2022), we explain the simulated differences in the aerosol spatial distribution between the models: CESM2 shows significantly faster shallow branches of the Brewer Dobson circulation facilitating transport of the relatively larger-sized aerosol to higher latitudes; UKESM shows a relatively isolated tropical pipe and older tropical age-of-air confining the relatively smaller-sized aerosols to the tropics; and the two GISS versions with either bulk or modal aerosol microphysics show elevated sulfate levels at higher latitudes as the result of smaller aerosol sizes and relatively stronger  
30 horizontal mixing (thus very young stratospheric age-of-air).

We then elucidate the role of these factors in driving the stratospheric responses to SAI. We find a large spread in the magnitudes of the tropical lower stratospheric warming amongst the models, which can be partially attributed to the



differences in aerosol distribution and sizes. Regarding the stratospheric ozone responses, we find a good agreement in the  
35 tropics between the models with modal microphysics, with lower stratospheric ozone changes consistent with the SAI-  
induced modulation of the large-scale circulation and the resulting changes in transport. In contrast to the relative agreement  
at low latitudes, we find a large inter-model spread in the Antarctic ozone responses that can largely be explained by the  
differences in the simulated latitudinal distributions of aerosols as well as the degree of implementation of heterogeneous  
halogen chemistry on sulfate. **Finally, we** also find large differences in stratospheric water vapour responses amongst the  
40 models, with CESM2 and GISS with modal microphysics both showing significant increases in stratospheric water vapour  
under SAI consistent with the increase in cold point temperatures that were largely not **reproduced** in UKESM.

For the GISS runs with bulk microphysics, the SAI simulations show contrastingly different stratospheric responses to the  
models using the modal aerosol treatment, including the absence of lower stratospheric warming as well as significant  
45 reductions in stratospheric water vapour and ozone. The results point towards the importance of detailed treatment of aerosol  
processes, although some problems in halogen chemistry in GISS are identified that require further attention. Overall, our  
results contribute to an increased understanding of the underlying physical mechanisms as well as the sources of uncertainty  
in model projections of climate impacts from SAI.

## 1. Introduction

50 Observations of the cooling produced by past explosive volcanic eruptions (Robock, 2000) have prompted numerous  
investigations into the feasibility and risks of artificially injecting SO<sub>2</sub> in the lower stratosphere in order to partially  
counteract the effect of rising greenhouse gases (Crutzen, 2006); this is usually termed Sulfate Aerosol **Injection** (SAI) or  
Solar Geoengineering. The formation of sulfate aerosols after SO<sub>2</sub> oxidation prevents a portion of the incoming sunlight  
from reaching the troposphere, thus cooling the surface. However, this is not the only effect that would be produced from  
55 sulfate aerosols in the Earth system (Vioni et al., 2021). The localized heating of the lower stratosphere would modify the  
local chemical composition of the atmosphere as well as alter the large-scale atmospheric circulation. These **side-effects** have  
been investigated in the past by various studies, which most often focused on one single model. For instance, Ferraro et al.  
(2015) analysed the impacts of a tropical sulfate injection on stratospheric dynamics in the University of Reading  
Intermediate General Circulation Model (IGCM). Tilmes et al. (2017, 2018a) and Richter et al. (2017) analysed the  
60 atmospheric response to injections at different latitudes and/or altitudes in the Community Earth System Model 1 (CESM1)  
with the Whole Atmosphere Community Climate Model (WACCM) as its atmospheric component (CESM1-WACCM) in  
order to understand the underlying mechanisms in the climate response.

However, models are themselves imperfect, and hence model intercomparisons are useful in understanding uncertainties in  
65 climate responses to SAI. Several of such intercomparison studies were carried out as a part of Geoengineering Model



Intercomparison Project (GeoMIP, Kravitz et al., 2011; 2015). However, the implementation of the experimental protocols often differed between the participating climate models, which hindered confident attribution of drivers of the intermodal spread. Pitari et al. (2014) found large differences in the simulated stratospheric ozone responses in the GeoMIP G4 experiment, which were partially related to different profiles of the latitudinal distribution of sulfate aerosols used in various models. Tilmes et al. (2022) examined the impacts of SAI on the future evolution of stratospheric ozone using the three Earth System Models (ESMs) with interactive chemistry participating in the GeoMIP G6 experiment. However, only two out of the three models included an interactive aerosol scheme while the third model prescribed the aerosol optical depth (AOD) from the G4SSA experiment (Tilmes et al., 2015). Moreover, even for these two models, both the location of injections (25 km at 0° for CESM and 10°S-10°N at 18 km in UKESM) and the yearly amounts of SO<sub>2</sub> injected (the injection rates were modified to achieve an amount of cooling corresponding to the model difference between the Shared Socioeconomic Pathway (SSP) 5-8.5 and 2-4.5 scenarios (Meineshausen et al., 2020) varied considerably.

Finally, rather than injecting fixed amounts of sulfur dioxide (SO<sub>2</sub>), a precursor to sulfate aerosol formation, some recent studies examined the climate response to SAI in CESM1-WACCM using a feedback algorithm that injected varied amounts of SO<sub>2</sub> at four off-equatorial locations in order to control not only the global mean surface temperature but also the equator-to-pole and inter-hemispheric temperature gradients (e.g. Tilmes et al., 2018b). This approach has been shown to result in a more uniform surface cooling and, thus, fewer side-effects than an equatorial injection strategy (Kravitz et al., 2019). Providing the basis for replicating this approach in other climate models is one of the goals of the experiments described here, as detailed in the companion paper (Visioni et al. (2022), hereafter PART1). Such a multi-model comparison will provide insights into the climatic impacts of a more complex, time-varying SAI strategy aimed at reducing some of the surface side effects of a potential deployment. However, understanding intermodel differences in the simulated responses in such experiments could present its own challenges due to likely different magnitudes and distributions of the simulated SO<sub>2</sub> injections amongst the models, and thus differences in the stratospheric responses and their contribution to the surface climate changes.

The study presented here avoids these issues by examining a set of carefully designed sensitivity experiments with fixed point injections of SO<sub>2</sub> in the lower stratosphere at single latitudes of either 30°S, 15°S, 0°, 15°N or 30°N. We use 3 comprehensive ESMs that were previously used to inform a range of past and future climate studies as well as participated in the CMIP6 intercomparison, i.e. CESM version 2 with WACCM6 as it's atmospheric component (CESM2-WACCM6), United Kingdom Earth System Model (UKESM1.0) and NASA Goddard Institute for Space Studies model (GISS-E2.1-G). By keeping the simulated SO<sub>2</sub> emissions in the model experiments as close as possible, we aim to robustly identify the similarities and differences in the simulated responses amongst the models, as well as identify and attribute the drivers of these differences. Such an exercise aims to improve our understanding of the sources of uncertainty in climate model projections of SAI response as well as identify areas of future model improvements. In addition, as mentioned above,



100 characterising model responses to fixed SO<sub>2</sub> injections and origins of inter-model differences will also help our understanding of the simulated responses in more complex scenarios of SAI deployment employing a feedback algorithm. PART1 analysed the simulated aerosol fields and their relationships to the surface temperature and precipitation responses in these experiments. Here we build on these findings by elucidating the contribution of biases in model transport alongside further illustrating aspects of aerosol microphysics. We then characterise the simulated changes in stratospheric and 105 tropospheric temperatures, ozone, water vapour and the large-scale circulation, elucidating the role of the above aspects to the SAI responses as well as identifying commonalities and differences in the simulated responses. By doing so, we also elucidate whether the key findings of Tilmes et al. (2018a) and Richter et al. (2017) utilizing CESM1-WACCM can be reproduced in a multi-model framework.

## 2. Methods

110 A detailed description of the ESMs used and the simulations performed can be found in **Part 1 of this study (PART1)**. Briefly, we use CESM2-WACCM6 (Gettelman et al., 2019, Danabasoglu et al., 2020, thereafter CESM2), UKESM1.0 (Sellar et al., 2019, Archibald et al., 2020; thereafter UKESM) and GISS-E2.1-G (Kelley et al., 2020). Both CESM2 and UKESM use modal aerosol microphysical schemes that account for the evolution of the aerosol size distribution. For GISS- 115 **Accumulation** aerosol modes (Bauer, et al., 2008; 2020; hereafter GISSmodal) and the bulk aerosol treatment **OMA** (Koch et al. 2006; hereafter GISSbulk) schemes; this allows us to test the importance of detailed representation of aerosol processes for the simulated response. With each of the models, we perform five simulations with constant single point injections of 12 Tg-SO<sub>2</sub>/yr at 22 km altitude and either 30°S, 15°S, 0°, 15°N, or 30°N latitude.

120 **The injections** are initialised in January 2035 from the first member of the CMIP6 SSP2-4.5 simulation for each model (Meineshausen, et al., 2020) and extend through December 2044 (**i.e.** 10 years in total). Since the focus of this paper is on the simulated atmospheric responses, we diagnose the responses using the last 8 years of each simulation, **i.e.** slightly longer time period than in PART1 in order to reduce the contribution from interannual variability to the diagnosed signals.

## 3. Results

### 125 3.1 . Stratospheric sulfate aerosols and the role of transport

**PART1 included a discussion of the simulated sulfate aerosol fields and their relationship to the aerosol microphysical schemes in the three ESMs. Below we summarise the main findings and build on them by elucidating the contribution of biases in model transport to the simulated aerosol spatial distributions.**



130 Figure 1 shows changes in sulfate **surface aerosol densities (SAD)** simulated in each run. Apart from providing a measure of  
the simulated sulfate burden, the diagnostic is particularly relevant for ozone chemistry, as it is directly related to the rates of  
heterogeneous reactions occurring on aerosol surfaces. Since the SAD diagnostic was not available for the two GISS model  
versions, we calculate SAD off-line for all models from the monthly-mean sulfate mass mixing ratios ( $\chi_i$ ), number  
concentrations ( $N_i$ ) and number densities ( $n_i$ ) using the formula in Eq. 1, with the mean radius ( $r_i$ ) in each of the aerosol  
135 modes calculated as given by Eq. 2: ( $\sigma_i$  denotes the prescribed geometric standard deviation for each mode and  $\rho$  the sulfate  
aerosol density)

$$SAD = \sum 4\pi r_i^2 n_i \exp(2\ln^2 \sigma_i) \quad (1)$$

$$r^3 = \frac{3}{4\pi \exp(4.5\ln^2 \sigma_i)} \cdot \frac{\chi_i}{\rho N_i} \quad (2)$$

140

**Note that the** resulting SAD changes are somewhat smaller in CESM2 and UKESM than the values obtained from the  
corresponding online SAD diagnostics (Fig. S1, Supplement), but for consistency we compare the off-line calculated values  
for all models.

145 For off-equatorial injections, aerosols are primarily dispersed across the hemisphere they were injected in, with little cross-  
over to the opposite hemisphere. Such limited dispersion into the opposite hemisphere to that of injection was also noted in  
simulations of explosive volcanic eruptions, although for higher injection rates at higher altitudes more significant cross-  
equatorial transport was noted (e.g. Jones et al., 2017). CESM2 simulates the largest sulfate SAD in the high latitudes out of  
the three ESMs with modal aerosol microphysics; these highest SAD values also correspond to the largest total sulfate loads  
150 in the mid- and high latitudes as shown in PART1. This can be explained by the significantly faster shallow branch of the  
Brewer-Dobson Circulation (BDC) simulated in CESM2 in both hemispheres (Fig. 2). The fast shallow branches of the  
BDC, found in the lower stratosphere (below ~30 hPa) and active year-round, facilitate transport of sulfate from the injection  
locations in the tropics to higher latitudes, resulting in significantly elevated mid- and high latitude sulfate loadings.

155 In the simulations with equatorial injections (third row in Fig. 1), the highest SAD are found in the tropics, with largest  
variability across the models in regions poleward of 30° latitude. UKESM shows greatest confinement of sulfate inside the  
tropical pipe out of the different models; the stronger confinement in UKESM is also visible for other injection locations.  
Comparison of the UKESM age-of-air (AoA) with MIPAS satellite observations (Stiller et al., 2020) shows significantly  
older model AoA in the tropics than observed (Fig. 3); this indicates a slow rate of transport out of the tropics and is this  
160 consistent with the high fraction of sulfate aerosols found at low latitudes. In addition, UKESM simulates the fastest vertical  
velocities in the tropics at the altitudes where sulfate aerosols are injected (~22 km, Fig. 4). This slows down the



gravitational settling of aerosols, thereby adding on to their tropical confinement. The effect is further amplified by the relatively smaller aerosol sizes in UKESM than in CESM2 (as indicated by the locally higher SAD in Fig. 1), with maximum effective radius of  $\sim 0.3 \mu\text{m}$  in UKESM compared to  $\sim 0.6 \mu\text{m}$  in CESM2.

165

Both GISSmodal and GISSbulk show a relatively deeper aerosol layer, i.e. the simulated sulfate SAD (Fig. 1) and sulfate aerosol concentrations (Fig. 3 in PART1) extend to higher altitudes. This is partially because of the much smaller size of sulfate aerosols, resulting in slower gravitational settling and increased lifetime of sulfate aerosols in the stratosphere. As shown in PART1, the maximum effective radius reaches  $\sim 0.25 \mu\text{m}$  in GISSmodal (compared to  $\sim 0.6 \mu\text{m}$  in CESM2) but the value drops substantially near the injection location corresponding to locally very small aerosol particles and very high SAD values (Fig. 1). The lack of an explicit aerosol nucleation model in CESM2, where nucleating aerosols are directly transferred to the Aitken mode, may help explain why such a drop is not present in CESM (see also Weinstein et al., 2022). In addition, the GISS model shows anomalously young AoA throughout the depth of tropical pipe when compared to observations (Fig. 3) but relatively slow resolved upwelling (Fig. 4), thus suggesting additional diffusion processes operating in the model that enhance transport of air (and aerosols) to higher altitudes by dispersion and/or mixing.

170  
175

Importantly, GISSbulk shows substantially (i.e. a few times) larger sulfate SAD than any other models with modal aerosol microphysics (Fig. 1, rightmost column). The bulk aerosol scheme restricts the mean size of aerosols (with the imposed dry radius of  $0.15 \mu\text{m}$ ), thereby preventing their growth by coagulation and leading to the formation of a large number of relatively small aerosols. These high sulfate concentrations are also readily transported to higher latitudes since smaller particle sizes have lower gravitational settling velocities and increased atmospheric lifetimes. In addition, horizontal mixing in GISS is likely very strong – this can be inferred from the anomalously young model AoA simulated throughout the stratosphere (Fig. 3<sup>1</sup>). In general, AoA shows combined effects of transport from the residual circulation and mixing (Garny et al, 2014). Since the residual circulation simulated in the two GISS models is generally comparable to that in UKESM and much weaker than in CESM (Fig. 2), the relatively younger AoA in GISS is mostly likely the result of much stronger mixing. This is further supported by the weaker climatological zonal winds simulated in GISS in the stratosphere in both hemispheres (Fig. S2) and, thus, weaker potential vorticity gradients that control mixing efficiency (Abalos and Camara, 2020). Neither of the two GISS models are able to simulate the Quasi-Biannual Oscillation (QBO), which is known to be an important factor in controlling the confinement of aerosols inside the tropical latitudes (Niemeier and Schmidt, 2017; Visioni et al., 2018)

180  
185  
190

---

<sup>1</sup> Fig. 3 includes the result of a historical GISSbulk experiment with prescribed observed sea surface temperatures and sea-ice. While the presence of interactive ocean component in the SAI GISSbulk integrations discussed in this work would have some impact on the resulting AoA simulated by the model, no analogous historical run was available for the model with interactive ocean.



### 3.2 Temperature

The absorption of incoming solar and outgoing terrestrial radiation by sulfate aerosols increases temperatures in the tropical lower stratosphere in the three models with modal aerosol microphysics (Fig. 5). The change occurs primarily in the tropics; however, both CESM2 and GISSmodal also show substantial temperature increase in the mid-latitude lower stratosphere in the hemisphere of injection. This is consistent with both models showing significant aerosol levels outside of the tropics (Section 3.1, Fig. 1; see also PART1). In each model, the magnitude of the response is largest for the equatorial injection case (Figure 5). For example, CESM2 simulations show tropical lower stratospheric warming of up to ~4-6 K for off-equatorial injections and up to ~8 K for the equatorial injection.

The magnitude of the lower stratospheric warming is approximately a factor of two smaller in UKESM than in CESM2. This can be partially understood by the smaller average size of sulfate aerosols (as can be inferred from SAD values in Fig. 1, see also PART1), which are less effective at absorbing terrestrial radiation (Laakso et al., 2022), and by the smaller total sulfate aerosol load (PART1). However, differences in the radiative codes are still an important contributing factor (e.g. Boucher et al., 1998; DeAngelis et al., 2015; Niemeier et al., 2020). For the equatorial injection case in UKESM, the strong confinement of sulfate inside the tropical pipe, and their uplift via the somewhat faster tropical velocities (Fig. 3), leads to a greater vertical extent of the lower stratospheric warming.

In GISSmodal, the lower stratospheric warming is comparable to CESM2 in terms of the maximum amplitude but much more vertically spread for all injection locations. As discussed in Section 3.1, this is related to a greater depth of the aerosol layer in GISSmodal, resulting from smaller sulfate particle sizes, thus slower gravitational settling, a weaker shallow branch of the BDC and likely stronger diffusion. In addition, the associated acceleration of tropical upwelling in the stratosphere from aerosol heating, which acts to increase adiabatic cooling and thus opposes the diabatic heating from aerosol absorption, is much smaller in GISSmodal than in CESM2 (Figure 6).

In contrast to the three models with a modal microphysics, no lower stratospheric warming is simulated in GISSbulk (Fig. 5, rightmost column). The use of a bulk aerosol scheme with fixed aerosol sizes results in much smaller particles than for the models with more complex modal aerosol schemes; the small aerosols are not as effective in absorbing radiation. In addition, the simulations are associated with substantial reductions in lower stratospheric ozone (Section 3.3), which otherwise contributes to the short-wave heating there (Richter et al., 2018); these thus effectively offset any warming tendency from aerosol absorption.

As expected, all models simulate tropospheric cooling as the result of the reduction of the incoming solar radiation from SAI. In each model, the strongest cooling is found in the hemisphere of injection, consistent with the near-surface



temperature changes discussed in PART1. In each case the cooling maximises in the tropical upper troposphere; this is  
225 consistent with changes produced by the strong radiative feedback from water vapour, the tropospheric concentrations of  
which decrease when the surface is cooled (Section 3.4). As the result, surface temperature signals tend to be amplified in  
the upper troposphere; this is also the case under global warming from rising greenhouse-gases (Sherwood et al., 2010;  
Steiner et al., 2020), and predicted by the moist adiabatic lapse rate theory (Stone and Carlson, 1979). However, here the  
230 magnitude of the tropospheric cooling varies substantially between the models, with the two GISS models showing strongest  
responses, consistent with the near-surface temperature changes discussed in PART1. A large difference in the upper  
tropospheric temperature responses amongst models has also been observed under climate change simulations (Minschwaner  
et al., 2006).

### 3.3. Ozone and large-scale circulation

#### 235 3.3.1. Tropics/mid-latitudes in models with modal microphysics

Changes in tropospheric and stratospheric temperatures and, hence, the large-scale transport as the result of SAI drive  
changes in stratospheric ozone. CESM2, UKESM and GISSmodal all show increased ozone in the tropical lower  
stratosphere at ~70 hPa (Figure 7). The response results from local deceleration of upwelling in the tropical troposphere  
(Figure 6) brought about by the increase in static stability associated with heating in the lower stratosphere and cooling in the  
240 troposphere (Fig. 5). This deceleration of tropospheric upwelling slows down the transport of ozone-poor tropospheric air  
into the lower stratosphere, thus increasing ozone in the region. The differences in the magnitudes of ozone responses  
amongst the three models with modal aerosol microphysics are commensurate with the differences in the lower stratospheric  
temperature responses, with larger ozone increases in GISSmodal and CESM2 and smaller in UKESM. As expected, we  
find a strong correlation between the lower stratospheric ozone and temperature responses across the models (Fig. S3),  
245 thereby supporting our understanding of the drivers of the ozone changes in the region.

At the altitudes above the lower stratospheric ozone increase, CESM2, UKESM and GISSmodal all show local ozone  
reductions near the latitude of SAI. The response can also be explained by the associated changes in the large-scale residual  
circulation. As shown in Fig. 6, tropical upwelling accelerates in the stratosphere under SAI, in particular near the latitude of  
250 injection, thus bringing more air with lower ozone mixing ratios higher up. In CESM2 and UKESM, there is also a further  
ozone increase above that and, for CESM2 only, at middle/higher latitudes, consistent with the enhanced transport of ozone  
from the production region (tropical middle stratosphere, i.e. where ozone mixing ratios maximize). The ozone increases in  
the high latitude middle stratosphere evident in CESM2 are not reproduced in UKESM because of the smaller changes in  
downwelling simulated in the model. **Note that although** the simulated tropical and mid-latitude ozone responses are  
255 primarily dynamically driven (by changes in ozone transport), any associated changes in chemistry (Tilmes et al, 2018) do



contribute to the simulated responses (Tilmes et al., 2022). In contrast to CESM2 and UKESM, GISSmodal shows a small ozone decrease of a few percent in the upper stratosphere; the response is consistent with the elevated ClO in the region (Fig. S4) and suggests problems in the chemistry scheme in GISS that merit further attention by the modelling teams.

260 When the ozone responses are integrated vertically over the whole atmosphere (Fig. 8), we find a reasonably good agreement between the tropical column ozone responses between CESM2 and UKESM. While there is some cancelation between the local ozone decrease at ~30 hPa and the ozone increase below, the reduction in ozone dominates and the simulations show local decreases in column ozone near the injection latitude of the order of ~10 DU. These tropical column ozone decreases are larger for UKESM, in particular for the equatorial injection case, consistent with a smaller increase in lowermost  
265 stratospheric ozone as the result of weaker warming discussed above. In the opposite hemisphere to the location of injection, both models show small but statistically significant increases in tropical ozone columns of a few DU as the result of changes in transport. In general, these tropical ozone changes, whilst small in absolute terms, can play a relatively important role given the much lower climatological column ozone values found in the tropics than at higher latitudes. A similar pattern of tropical column O<sub>3</sub> responses was also found in GISSmodal, although the column O<sub>3</sub> changes there tend to be more negative,  
270 presumably because of the contribution of the reductions in upper stratospheric ozone (the origins of which in this model, as discussed above, are not fully understood and suggest problems in the chemistry scheme).

### 3.3.2. Antarctic stratosphere

In the Southern Hemisphere (SH) high latitudes, CESM2 shows a significant ozone decrease in the lower stratosphere, in particular for the SH injections (up to ~35% ozone decrease in the polar lowermost stratosphere, Fig. 7, or up to ~50 DU  
275 vertically averaged, Fig. 8). These yearly mean changes are dominated by the response during austral spring (Fig. S6 and Fig. 8). As discussed in Section 3.1., CESM2 has a very fast shallow BDC, which effectively transports sulfate aerosols from the SO<sub>2</sub> injection locations in the tropics to higher latitudes. The presence of increased surface area densities in polar regions (Fig. 1) facilitates heterogenous halogen reactions inside the cold polar vortex that convert halogen species from their reservoir forms into active species like ClO or BrO (Figure S4 and Figure S5); these then enhance catalytic ozone  
280 destruction during austral spring. 

A similar decrease in the SH lower stratospheric ozone is not reproduced in UKESM in the yearly mean (Fig. 7). The model also does not show any significant Antarctic ozone depletion during austral spring (Fig. 8 and Fig. S6). **First**, UKESM shows greater confinement of sulfate aerosols inside the tropical pipe and weaker shallow BDC than CESM2 (Sect. 3.1). Therefore,  
285 the model simulates much lower aerosol concentrations at high latitudes (Fig. 1). **Second**, UKESM does not include the important heterogenous ClONO<sub>2</sub> + HCl reaction on sulfate aerosols, nor any heterogenous bromine chemistry on sulfate aerosols. Both effects significantly reduce the concentrations of activated halogens simulated in the lower stratosphere under SAI (Fig. S4 and Fig. S5), which thus limits the amount of catalytic ozone depletion in the Antarctic lower stratosphere.



290 **We note that, in** general, the magnitude of the chemical response depends on the background stratospheric halogen  
concentrations, which are projected to decrease over the 21<sup>st</sup> century, and thus any halogen-catalysed ozone reduction from  
SAI would be lower in later parts of the century (Tilmes et al., 2021). Similar considerations will also apply to the impacts of  
SAI on the Arctic ozone; however, the short length of the simulations (i.e. 8 years analysed) does not **allow to** assess this  
confidently, as any changes in ozone in the NH high latitudes will be dominated by natural interannual variability.

295

In comparison, the modal version of GISS also show decreases of Antarctic ozone in the lower stratosphere coinciding with  
local increases in ClO (Figure S4). However, the coupled O<sub>3</sub>-ClO response is qualitatively and quantitatively similar for all  
injection cases (despite large differences in the high latitude sulfate levels), suggesting that factors other than the latitudinal  
distribution of sulfate and, thus, of anomalous heterogenous halogen activation on sulfate surfaces, could be an important  
300 contributing driver in the model.

### 3.3.3. Tropospheric ozone changes

In addition to the stratospheric ozone changes in GISSmodal, the model also shows reductions of tropospheric ozone (up to  
~15%) throughout of most of the troposphere. The response could be related to the significantly stronger tropospheric  
cooling (Fig. 5) and thus a stronger reduction in tropospheric water vapour (Fig. 10), which plays an important role in  
305 tropospheric ozone production. The response is not reproduced in either CESM2 or UKESM, which could be because of the  
smaller level of tropospheric cooling in these models. In addition, the CESM2 **version used** includes a chemistry scheme  
tailored for middle atmosphere studies and, thus, does not include comprehensive tropospheric chemistry; this factor thus  
likely played a role in determining the tropospheric ozone response simulated in the model.

### 3.3.4. Response in GISS model with bulk aerosol microphysics

310 In stark contrast to the ozone responses in the three models with modal aerosol microphysics, the bulk version of GISS  
simulates substantial reductions of lower stratospheric ozone throughout the globe (locally up to 40-60 %, Fig. 8). The  
response is likely related to the number and size of sulfate aerosols produced from SO<sub>2</sub> injections, i.e. to the very high  
concentrations of very small aerosols simulated in GISSbulk. Since smaller aerosols have proportionally larger surface areas  
than their larger counterparts, this leads to much higher sulfate SAD compared to the modal version of GISS (Fig. 1). In  
315 addition, smaller aerosols have longer lifetimes, and can also be transported rapidly by the presumed strong mixing in the  
model (Section 3.1). All of these factors lead to significantly elevated sulfate SAD simulated in GISSbulk throughout the  
lower stratosphere. These could in principle enhance heterogenous halogen activation and, thus, produce substantial ozone  
depletion in these runs. **We note, however, that the** simulations do not show elevated active halogen concentrations in the  
lower stratosphere (the simulated lower stratospheric ClO and BrOx levels in fact decrease under SAI in GISSbulk, Fig. S4



320 and S5) but only spurious increases in ClO at higher altitudes, highlighting problems in the chemistry scheme in GISS that merit future attention.

### 3.4 Stratospheric water vapour

Figure 9 shows the associated changes in water vapour. We find large differences in the stratospheric water vapor (SWV) responses amongst the models. SWV increases in CESM2 and GISSmodal for all injection locations, consistent with the  
325 increase in cold point tropopause temperatures resulting from the warming of the lower stratosphere. The increase in SWV is strongest in the simulations with equatorial injections, consistent with the largest magnitude of the lower stratospheric warming (Section 3.2, Fig. 5). However, the increase in SWV in CESM2 is simulated throughout the entire stratosphere, while the GISSmodal simulations show negative SWV changes in the upper stratosphere, especially at high latitudes; the latter may be related to its problems with halogen chemistry there (see Section 3.3.).

330

The large increase in SWV under SAI is not reproduced in UKESM, which does not show large changes in SWV in any of the experiments except for the equatorial injection case. In fact, instead of an increase in SWV seen in CESM and GISSmodal, there is a very small decrease in SWV for simulations with injections at 30°S and 30°N. This may be related to anomalously high climatological SWV in that model (Archibald et al., 2020). The increase in stratospheric water vapour  
335 under SAI is also not reproduced in the GISSbulk simulations, which show decreases of SWV consistent with the absence of warming in the lower stratosphere. However, in all simulations carried out with the four models water vapor decreases in the troposphere as the result of surface and tropospheric cooling, with the largest changes found in for GISSbulk.

Apart from the differences in the SAI responses amongst the models, we also find large differences in the climatological  
340 SWV values (contours in Fig. 9). These differences are consistent with the large inter-model spread in SWV reported amongst all CMIP6 model (Keeble et al., 2021).

### 3.5 Zonal winds

Figure 10 shows changes in zonal winds resulting from SAI. Note that both CESM2 and UKESM include an internally generated QBO, whilst the two GISS models do not. The equatorial SO<sub>2</sub> injection in CESM2 and UKESM leads to a  
345 westerly response in the tropical lower stratosphere and an easterly response above. This pattern corresponds to a locking of the QBO in a permanent westerly phase (Fig. S7; see also e.g. Aquila et al., 2014; Jones et al., 2022) and arises because of the acceleration of equatorial upwelling under SAI (Fig. 6) inhibiting the downward propagation of the westerly QBO shear (Franke et al., 2021). A similar response was also found for UKESM in G6 GeoMIP experiment (Jones et al., 2022). The QBO locking is not reproduced for the 15° and 30° injection cases in CESM2 and UKESM (Fig. S7); this is because the  
350 acceleration of tropical upwelling occurs off-equatorial near the injection latitudes (Fig. 6). The results illustrate that off-



equatorial injections successfully avoid QBO locking, in agreement with Kravitz et al., (2019). Since two GISS models do not include any representation of the QBO, zonal wind is always easterly in the entire tropical stratosphere (Fig. S7).

355 In the extra-tropical stratosphere, CESM2, UKESM and GISSmodal all simulate strengthening of stratospheric jets in both hemispheres, consistent with geostrophic balance and the strengthening of the horizontal temperature gradient brought about from heating in the lower stratosphere. However, the derived responses are subject to a lot of interannual variability due to short length of the integrations, which prevent confident analysis of any inter-model differences. Unlike the three models with modal microphysics, GISSbulk shows weakening of zonal winds in the lower stratosphere and the free troposphere below, consistent with the tropical tropospheric cooling simulated in the model.

360

In the troposphere, however, i.e. where the interannual variability is lower, all models suggest qualitatively consistent impacts on the tropospheric jets. In particular, the off-equatorial injection cases suggest an equatorward shift of the tropospheric jet in the hemisphere of injection and an opposite-sign response in the other hemisphere. In the case of equatorial injections, tropospheric jets weaken in both hemispheres. The qualitative agreement between GISSbulk, which does not show a warming in the tropical lower stratosphere, and the other three models illustrates the role of changes in meridional temperature gradients within the troposphere in contributing to the simulated changes in tropospheric jets.

365

#### 4. Summary and Discussion

This paper constitutes Part 2 of a study performing a first systematic inter-model comparison of atmospheric responses to equatorial and off-equatorial stratospheric sulfate aerosol injections. We used three comprehensive Earth System Models - CESM2-WACCM6, UKESM1.0, and GISS-E2.1-G; for the latter we used two model versions, one with modal and one with bulk aerosol microphysics, to illustrate the importance of a detailed treatment of aerosol processes. We performed a set of five sensitivity experiments with constant point injections of 12 Tg-SO<sub>2</sub>/yr in the lower stratosphere at either 30° S, 15° S, 0°, 15° N or 30° N.

370

375 Building on Part 1 of this study, we demonstrated how inter-model differences in the simulated sulfate aerosol fields relate to biases in the climatological circulation and specific aspects of the model microphysics. In particular, CESM2 was found to simulate the highest concentrations of sulfate aerosols in the high latitudes than the other two models with modal microphysics. This could be understood in light of the significantly faster shallow branch of the Brewer Dobson circulation in CESM2, and a relatively isolated tropical pipe and older tropical age-of-air in UKESM. The two GISS versions also simulated elevated sulfate surface area densities at higher latitudes, consistent with smaller sizes of aerosol particles and relatively stronger horizontal mixing (thus very young stratospheric age-of-air).

380



We then further elucidated the role of these factors in driving the SAI responses. A large spread in the magnitudes of the tropical lower stratospheric warming was found amongst the models, and these could partially be attributed to the differences in aerosol distributions and their sizes. Whilst differences in radiative parametrizations certainly also played an important role, those are harder to isolate and would require further sensitivity experiments (e.g. with fixed size distribution and specified chemistry). For each model, the strongest lower stratospheric warming was found for the equatorial injection case, in agreement with previous simulations (e.g. Kravitz et al., 2019). Regarding the associated stratospheric ozone responses, all models with modal aerosol microphysics were found to agree in the tropical and subtropical latitudes. The ozone response there could be explained by the associated changes in upwelling and the large-scale Brewer-Dobson circulation, and were thus commensurate in magnitude to the associated changes in lower stratospheric temperatures amongst the models. These lower stratospheric ozone changes gave rise to local decreases in total column ozone near the latitude of injection and small increases in the tropical/subtropical regions further away.

In contrast to the relative agreement amongst the models in ozone responses at low latitudes, we found a large inter-model spread in the Antarctic ozone responses; these could largely be explained by the differences in the simulated latitudinal distributions of sulfate noted above as well as the degree of implementation of heterogeneous halogen chemistry on sulfate amongst the models. In particular, CESM2 simulated elevated surface area densities in the high latitudes; these facilitated heterogeneous halogen reactions that accelerated catalytic springtime ozone destruction in the Antarctic stratosphere. A similar response was not simulated in the UKESM model, consistent with a stronger confinement of sulfate aerosols inside the tropical pipe as well as an incomplete treatment of heterogeneous halogen chemistry on sulfate in the model version used. For stratospheric water vapour, the study found very large differences in the responses to sulfate injections amongst the models. CESM2 and GISS modal both showed substantial increases in stratospheric water vapour consistent with the increases in the tropical cold point temperatures. The response was not reproduced in UKESM, which only showed large increase in stratospheric water vapour in the equatorial injection case, or in GISS bulk, where stratospheric water vapour decreased as the result of absence of lower stratospheric warming. The latter is consistent with the GISS response reported in Pitari et al. (2014).

Our findings illustrate the importance of realistic representation of a range of microphysical, dynamical and chemical processes in models for accurately representing the potential impacts from SAI, both directly in the stratosphere as well as lower down at the surface. They also highlight the large uncertainties in the representation of these processes in Earth System Models. This thus suggests that certain degree of caution is needed in interpreting the results of studies conducted with individual models, and that more work should be undertaken to improve the models and evaluate them against the available observational data. For modelling intercomparisons, understanding and attributing the reasons behind the inter-model spread rather than focusing only on the multi-model mean responses would help identify areas in need of potential future model development, and thus narrowing the uncertainties in future model projections of SAI impacts.



In general, the sensitivity simulations with GISS using bulk treatment of aerosol processes illustrate the importance of detailed treatment of aerosol processes. In particular, the simulations with GISS bulk model showed very high sulfate surface area densities as the result of **the very small aerosol sizes**; these were in turn associated with changes in stratospheric ozone (including substantial reductions in lower stratosphere of up to ~40-60 %), temperatures, water vapour and zonal winds that contrasted strongly with the other models using modal aerosol microphysics. While problems in the halogen chemistry were identified that require further assessment by the modelling teams, the results point towards the importance of detailed treatment of aerosol microphysics, including resolving the complex relationships between the size distributions of aerosols and their physical and chemical properties, for accurate modelling of climate impacts from SAI. The importance of a detailed treatment of aerosol microphysics for the simulated SAI responses was also recently highlighted by Laakso et al. (2022), where multiple injection scenarios were simulated with the same model using two different microphysical schemes (in this case a modal and a sectional scheme). The resulting differences in simulated aerosol size distributions led to varying estimates of the overall radiative forcing produced by SAI.

Furthermore, by demonstrating the role of biases in climatological circulation, our results highlight the importance of not only model microphysics but also transport processes for simulating the evolution of the aerosol plume. This highlights the need for realistic representation of both aspects in models for determining the aerosol response and, thus, the potential impacts of SAI on atmospheric radiative balance, composition and circulation. Overall, our results contribute to an increased understanding of the underlying physical mechanisms as well as sources of uncertainty in model projections of climate impacts from SAI.

Finally, the results illustrate the dependence of the dynamical response to SAI on the latitude of SO<sub>2</sub> injections. For example, CESM2 and UKESM both showed that off-equatorial injections **avoid locking of the QBO in a perpetual westerly phase** that was otherwise found for the equatorial injection case. In the troposphere, all models suggested qualitatively similar impacts on tropospheric jets, i.e. equatorward shift of the tropospheric jet in the hemisphere of injection and an opposite-sign response in the other hemisphere. However, given the short length of the simulations detailed analysis of the dynamical response and the underlying mechanisms is beyond the scope of this study, but should be explored in the future with longer simulations.

445

### Acknowledgements

The Community Earth System Model (CESM) project is supported primarily by the National Science Foundation. We would like to acknowledge high-performance computing support from Cheyenne (<https://doi.org/10.5065/D6RX99HX>) provided



by NCAR's Computational and Information Systems Laboratory, sponsored by the National Science Foundation. The  
450 UKESM simulations were carried out using MONSooN2, a collaborative High-Performance Computing facility funded by  
the Met Office and the Natural Environment Research Council.

Support was provided by the Atkinson Center for a Sustainable Future at Cornell University for EMB, DV and DGM; and by  
the National Science Foundation through agreement CBET-1818759 for DV and DGM. Support for BK was provided in part  
455 by the National Science Foundation through agreement CBET-1931641, the Indiana University Environmental Resilience  
Institute, and the Prepared for Environmental Change Grand Challenge initiative. AJ and JMH were supported by the Met  
Office Hadley Centre Climate Programme funded by BEIS and by SilverLining through its Safe Climate Research Initiative.  
This material is based upon work supported by the National Center for Atmospheric Research, which is a major facility  
sponsored by the National Science Foundation under Cooperative Agreement no. 1852977.

#### 460 **Data Availability Statement**

The output from model simulations will be deposited in Cornell University eCommons library upon acceptance of the  
manuscript.

#### **Authors' contributions**

EMB performed the analysis and wrote the manuscript. DV performed the CESM simulations and helped with the discussion  
465 of the results and writing of the manuscript. BK performed the GISS simulations. AJ performed the UKESM simulations.  
All authors contributed to the discussion of the results and writing of the manuscript.

#### **Competing interests**

The authors declare no competing interests.

#### 470 **References**

- Abalos, M., & de la Cámara, A. (2020). Twenty-first century trends in mixing barriers and eddy transport in the lower  
stratosphere. *Geophysical Research Letters*, 47, e2020GL089548.
- Aquila, V., Garfinkel, C., Newman, P., Oman, L., and Waugh, D.: Modifications of the quasi-biennial oscillation by a  
475 geoengineering perturbation of the stratospheric aerosol layer, *Geophys. Res. Lett.*, 41, 1738–1744, 2014.



Archibald, A. T., O'Connor, F. M., Abraham, N. L., Archer-Nicholls, S., Chipperfield, M. P., Dalvi, M., Folberth, G. A., Dennison, F., Dhomse, S. S., Griffiths, P. T., Hardacre, C., Hewitt, A. J., Hill, R. S., Johnson, C. E., Keeble, J., Köhler, M. O., Morgenstern, O., Mulcahy, J. P., Ordóñez, C., Pope, R. J., Rumbold, S. T., Russo, M. R., Savage, N. H., Sellar, A., 380 Stringer, M., Turnock, S. T., Wild, O., and Zeng, G.: Description and evaluation of the UKCA stratosphere–troposphere chemistry scheme (StratTrop vn 1.0) implemented in UKESM1, *Geosci. Model Dev.*, 13, 1223–1266, <https://doi.org/10.5194/gmd-13-1223-2020>, 2020.

Bauer, S. E., Wright, D. L., Koch, D., Lewis, E. R., McGraw, R., Chang, L.-S., Schwartz, S. E., and Ruedy, R.: MATRIX (Multiconfiguration Aerosol TRacker of mIXing state): an aerosol microphysical module for global atmospheric models, 485 *Atmos. Chem. Phys.*, 8, 6003–6035, <https://doi.org/10.5194/acp-8-6003-2008>, 2008.

Bauer, S. E., Tsigaridis, K., Faluvegi, G., Kelley, M., Lo, K. K., & Miller, R. L., et al. (2020). Historical (1850–2014) aerosol evolution and role on climate forcing using the GISS ModelE2.1 contribution to CMIP6. *Journal of Advances in Modeling Earth Systems*, 12, e2019MS001978. <https://doi.org/10.1029/2019MS001978>, 2020.

490 Boucher, O., S.E. Schwartz, T.P. Ackerman, T.L. Anderson, B. Bergstrom, B. Bonnel, P. Chylek, A. Dahlback, Y. Fouquart, Q. Fu, R.N. Halthore, J.M. Haywood, T. Iversen, S. Kato, S. Kinne, A. Kirkevåg, K.R. Knapp, A. Lacis, I. Laszlo, M.I. Mishchenko, S. Nemesure, V. Ramaswamy, D.L. Roberts, P. Russell, M.E. Schlesinger, G.L. Stephens, R. Wagener, M. Wang, J. Wong, and F. Yang: Intercomparison of models representing direct shortwave radiative forcing by sulfate aerosols. 495 *J. Geophys. Res.*, 103, 16979–16998, doi:10.1029/98JD00997, 1998.

Crutzen, P.J. Albedo Enhancement by Stratospheric Sulfur Injections: A Contribution to Resolve a Policy Dilemma?. *Climatic Change* 77, 211, <https://doi.org/10.1007/s10584-006-9101-y>, 2006.

500 Danabasoglu, G., Lamarque, J.-F., Bacmeister, J., Bailey, D. A., DuVivier, A. K., Edwards, J., et al..The Community Earth System Model Version 2 (CESM2). *Journal of Advances in Modeling Earth Systems*, 12, e2019MS001916. <https://doi.org/10.1029/2019MS001916>, 2020.

DeAngelis, A., Qu, X., Zelinka, M. et al. An observational radiative constraint on hydrologic cycle intensification. *Nature* 505 528, 249–253, <https://doi.org/10.1038/nature15770>, 2015.

Ferraro, A. J., Charlton-Perez, A. J., & Highwood, E. J., Stratospheric dynamics and midlatitude jets under geoengineering with space mirrors and sulfate and titania aerosols. *Journal of Geophysical Research: Atmospheres*, 120(2), 414–429, 2015.



510 Franke, H., Niemeier, U., and Visioni, D.: Differences in the quasi-biennial oscillation response to stratospheric aerosol  
modification depending on injection strategy and species, *Atmos. Chem. Phys.*, 21, 8615–8635, <https://doi.org/10.5194/acp-21-8615-2021>, 2021.

515 Garny, H., Birner, T., Bonisch, H., and Bunzel, F.: The effects of mixing on age of air, *Journal of Geophysical Research-Atmospheres*, 119, 7015-7034, [10.1002/2013jd021417](https://doi.org/10.1002/2013jd021417), 2014.

520 Gettelman, A., Mills, M. J., Kinnison, D. E., Garcia, R. R., Smith, A. K., Marsh, D. R., Tilmes, S., Vitt, F., Bardeen, C. G.,  
McInerney, J., Liu, H.-L., Solomon, S. C., Polvani, L. M., Emmons, L. K., Lamarque, J.-F., Richter, J. H., Glanville, A. S.,  
Bacmeister, J. T., Phillips, A. S., Neale, R. B., Simpson, I. R., DuVivier, A. K., Hodzic, A., and Randel, W. J.: The Whole  
Atmosphere Community Climate Model Version 6 (WACCM6), *Journal of Geophysical Research: Atmospheres*, 124, 12  
380–12 403, <https://doi.org/10.1029/2019JD030943>, 2019.

525 Jones, A., Haywood, J. M., Scaife, A. A., Boucher, O., Henry, M., Kravitz, B., Lurton, T., Nabat, P., Niemeier, U., Séférian,  
R., Tilmes, S., and Visioni, D.: The impact of stratospheric aerosol intervention on the North Atlantic and Quasi-Biennial  
Oscillations in the Geoengineering Model Intercomparison Project (GeoMIP) G6sulfur experiment, *Atmos. Chem. Phys.*, 22,  
2999–3016, <https://doi.org/10.5194/acp-22-2999-2022>, 2022.

Jones AC, Haywood JM, Dunstone N, Emanuel K, Hawcroft MK, Hodges KI, Jones A. Impacts of hemispheric solar  
geoengineering on tropical cyclone frequency. *Nat Commun.*, 8(1):1382. doi: 10.1038/s41467-017-01606-0, 2017.

530 Keeble, J., Hassler, B., Banerjee, A., Checa-Garcia, R., Chiodo, G., Davis, S., Eyring, V., Griffiths, P. T., Morgenstern, O.,  
Nowack, P., Zeng, G., Zhang, J., Bodeker, G., Burrows, S., Cameron-Smith, P., Cugnet, D., Danek, C., Deushi, M.,  
Horowitz, L. W., Kubin, A., Li, L., Lohmann, G., Michou, M., Mills, M. J., Nabat, P., Olivieri, D., Park, S., Seland, Ø., Stoll,  
J., Wieners, K.-H., and Wu, T.: Evaluating stratospheric ozone and water vapour changes in CMIP6 models from 1850 to  
2100, *Atmos. Chem. Phys.*, 21, 5015–5061, <https://doi.org/10.5194/acp-21-5015-2021>, 2021.

535 Kelley, M., Schmidt, G. A., Nazarenko, L. S., Bauer, S. E., Ruedy, R., & Russell, G. L., et al.: GISS-E2.1: Configurations  
and climatology. *Journal of Advances in Modeling Earth Systems*, 12, e2019MS002025.  
<https://doi.org/10.1029/2019MS002025>, 2020.

540 Koch, D., Schmidt, G. A., and Field, C. V.: Sulfur, sea salt, and radionuclide aerosols in GISS ModelE, *Journal of  
Geophysical Research: Atmospheres*, 111, <https://doi.org/10.1029/2004JD005550>, 2006.



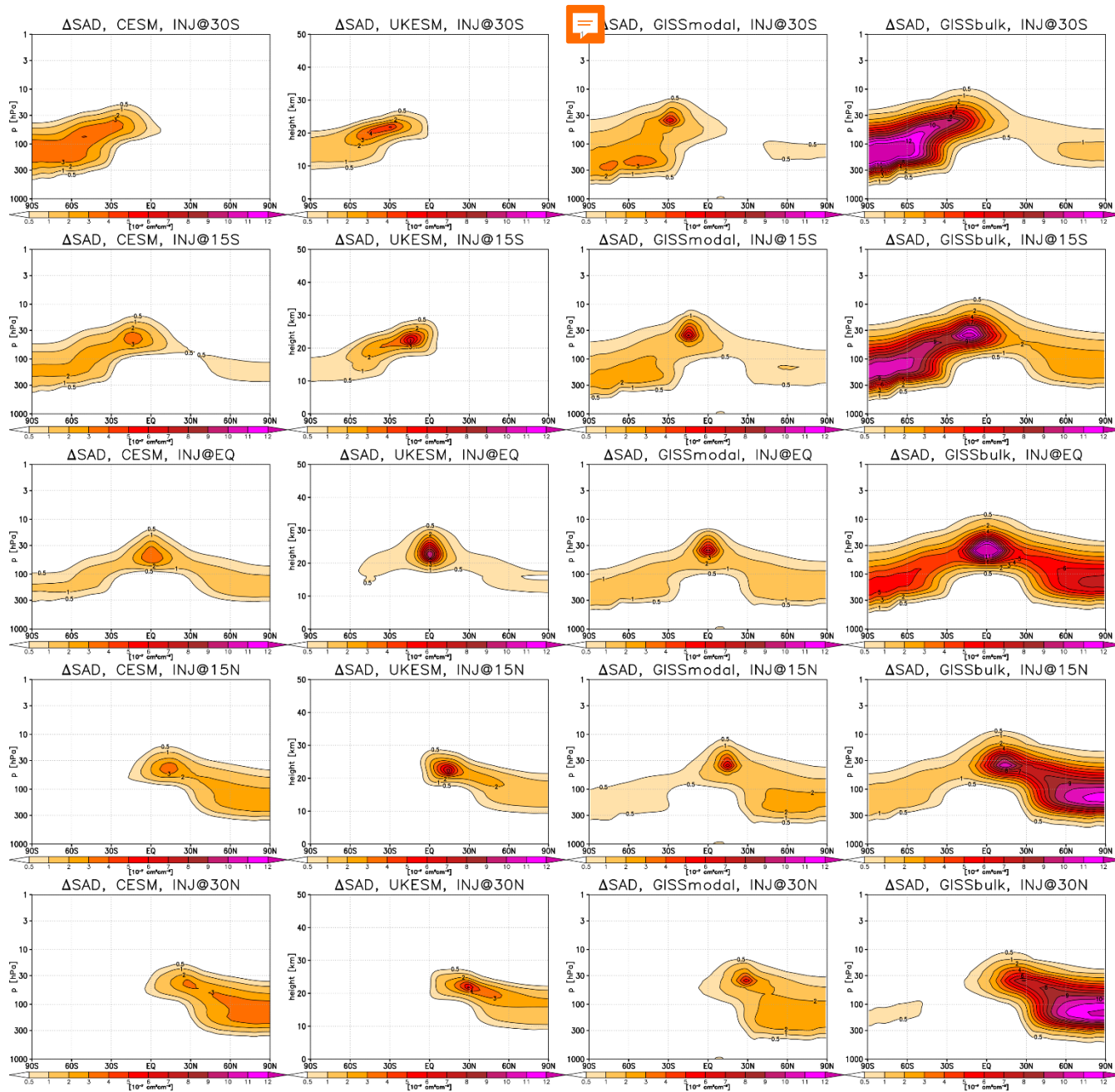
- Kravitz, B., Robock, A., Boucher, O., Schmidt, H., Taylor, K. E., Stenchikov, G., and Schulz, M.: The Geoengineering Model Intercomparison Project (GeoMIP), *Atmospheric Science Letters*, 12, 162–167, <https://doi.org/10.1002/asl.316>, 2011.
- 545 Kravitz, B., A. Robock, S. Tilmes, O. Boucher, J. M. English, P. J. Irvine, A. Jones, M. G. Lawrence, M. MacCracken, H. Muri, J. C. Moore, U. Niemeier, S. J. Phipps, J. Sillmann, T. Storelvmo, H. Wang, and S. Watanabe: The Geoengineering Model Intercomparison Project Phase 6 (GeoMIP6): Simulation design and preliminary results, *Geoscientific Model Development*, 8, 3379–3392, doi:10.5194/gmd-8-3379-2015, 2015.
- 550 Kravitz, B., MacMartin, D. G., Tilmes, S., Richter, J. H., Mills, M. J., Cheng, W., et al.. Comparing surface and stratospheric impacts of geoengineering with different SO<sub>2</sub> injection strategies. *Journal of Geophysical Research: Atmospheres*, 124(14), 7900–7918, 2019
- Laakso, A., Niemeier, U., Visioni, D., Tilmes, S., and Kokkola, H.: Dependency of the impacts of geoengineering on the stratospheric sulfur injection strategy – Part 1: Intercomparison of modal and sectional aerosol modules, *Atmos. Chem. Phys.*, 22, 93–118, <https://doi.org/10.5194/acp-22-93-2022>, 2022.
- 555 Meinshausen, M., Nicholls, Z. R. J., Lewis, J., Gidden, M. J., Vogel, E., Freund, M., Beyerle, U., Gessner, C., Nauels, A., Bauer, N., Canadell, J. G., Daniel, J. S., John, A., Krummel, P. B., Luderer, G., Meinshausen, N., Montzka, S. A., Rayner, P. J., Reimann, S., Smith, S. J., van den Berg, M., Velders, G. J. M., Vollmer, M. K., and Wang, R. H. J.: The shared socio-economic pathway (SSP) greenhouse gas concentrations and their extensions to 2500, *Geosci. Model Dev.*, 13, 3571–3605, <https://doi.org/10.5194/gmd-13-3571-2020>, 2020.
- 560 Minschwaner, K., A. E. Dessler, and P. Sawaengphokhai, Multimodel analysis of the water vapor feedback in the tropical upper troposphere, *J. Clim.*, 19, 5455–5464, 2006.
- Niemeier, U. and Schmidt, H.: Changing transport processes in the stratosphere by radiative heating of sulfate aerosols, *Atmos. Chem. Phys.*, 17, 14871–14886, <https://doi.org/10.5194/acp-17-14871-2017>, 2017.
- 570 Niemeier, U., Richter, J. H., and Tilmes, S.: Differing responses of the quasi-biennial oscillation to artificial SO<sub>2</sub> injections in two global models, *Atmos. Chem. Phys.*, 20, 8975–8987, <https://doi.org/10.5194/acp-20-8975-2020>, 2020.
- Pitari, G., Aquila, V., Kravitz, B., Robock, A., Watanabe, S., Cionni, I., Luca, N. D., Genova, G. D., Mancini, E., and Tilmes, S.: Stratospheric ozone response to sulfate geoengineering: Results from the Geoengineering Model Intercomparison Project (GeoMIP), *J. Geophys. Res.-Atmos.*, 119, 2629–2653, <https://doi.org/10.1002/2013JD020566>, 2014.
- 575



- Richter, J. H., Tilmes, S., Mills, M. J., Tribbia, J., Kravitz, B., MacMartin, D. G., Lamarque J.-F., Stratospheric dynamical response and ozone feedbacks in the presence of SO<sub>2</sub> injections. *Journal of Geophysical Research: Atmospheres*, 122, 12,557–12,573. <https://doi.org/10.1002/2017JD026912>, 2017.
- 580
- Sellar, A. A., Jones, C. G., Mulcahy, J. P., Tang, Y., Yool, A., Wiltshire, A., O'Connor, F. M., Stringer, M., Hill, R., Palmieri, J., Woodward, S., de Mora, L., Kuhlbrodt, T., Rumbold, S. T., Kelley, D. I., Ellis, R., Johnson, C. E., Walton, J., 505 Abraham, N. L., Andrews, M. B., Andrews, T., Archibald, A. T., Berthou, S., Burke, E., Blockley, E., Carslaw, K., Dalvi, M., Edwards, J., Folberth, G. A., Gedney, N., Griffiths, P. T., Harper, A. B., Hendry, M. A., Hewitt, A. J., Johnson, 585 B., Jones, A., Jones, C. D., Keeble, J., Liddicoat, S., Morgenstern, O., Parker, R. J., Predoi, V., Robertson, E., Siahann, A., Smith, R. S., Swaminathan, R., Woodhouse, M. T., Zeng, G., and Zerroukat, M.: UKESM1: Description and evaluation of the U.K. Earth System Model, *J. Adv. Model. Earth Sy.*, 11, 4513–4558, <https://doi.org/10.1029/2019MS001739>, 2019.
- Sherwood, S. C., W. Ingram, Y. Tsushima, M. Satoh, M. Roberts, P. L. Vidale, and P. A. O’Gorman, Relative humidity changes in a warmer climate, *J. Geophys. Res.*, 115, D09104, doi:10.1029/2009JD012585, 2010.
- 590
- Steiner, A. K., Ladstädter, F., Randel, W. J., Maycock, A. C., Fu, Q., Claud, C., Gleisner, H., Haimberger, L., Ho, S.-P., Keckhut, P., Leblanc, T., Mears, C., Polvani, L. M., Santer, B. D., Schmidt, T., Sofieva, V., Wing, R., & Zou, C.-Z., Observed Temperature Changes in the Troposphere and Stratosphere from 1979 to 2018, *Journal of Climate*, 33(19), 8165-8194, 2020.
- 595
- Stone, P. H., & Carlson, J. H., Atmospheric Lapse Rate Regimes and Their Parameterization, *Journal of Atmospheric Sciences*, 36(3), 415-423., 1979.
- Tilmes, S., Mills, M. J., Niemeier, U., Schmidt, H., Robock, A., Kravitz, B., Lamarque, J.-F., Pitari, G., and English, J. M.: 600 A new Geoengineering Model Intercomparison Project (GeoMIP) experiment designed for climate and chemistry models, *Geosci. Model Dev.*, 8, 43–49, <https://doi.org/10.5194/gmd-8-43-2015>, 2015.
- Tilmes, S., H., Richter J., J., Mills M., B., Kravitz, G., MacMartin D., F., Vitt, Lamarque J.-F. Sensitivity of aerosol distribution and climate response to stratospheric SO<sub>2</sub> injection locations. *Journal of Geophysical Research: Atmospheres*, 605 122, 12,591–12,615. <https://doi.org/10.1002/2017JD026888>, 2017.
- Tilmes, S., Richter, J. H., Mills, M. J., Kravitz, B., MacMartin, D. G., Garcia, R. R., et al. Effects of different stratospheric SO<sub>2</sub> injection altitudes on stratospheric chemistry and dynamics. *Journal of Geophysical Research: Atmospheres*, 123, 4654–4673. <https://doi.org/10.1002/2017JD028146>, 2018a.
- 610

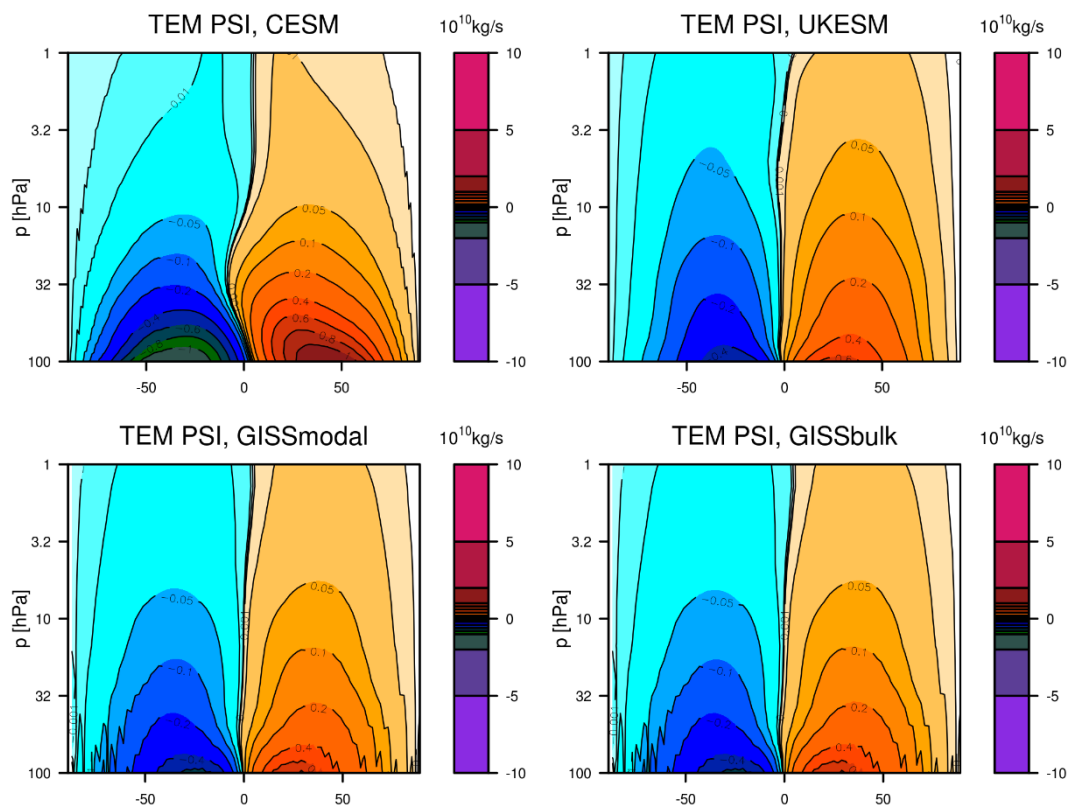


- Tilmes, S., Richter, J. H., Kravitz, B., MacMartin, D. G., Mills, M. J., Simpson, I. R., Glanville, A. S., Fasullo, J. T., Phillips, A. S., Lamarque, J.-F., Tribbia, J., Edwards, J., Mickelson, S., and Ghosh, S.: CESM1(WACCM) Stratospheric Aerosol Geoengineering Large Ensemble Project, *B. Am. Meteorol. Soc.*, 99, 2361–2371, <https://doi.org/10.1175/BAMS-D-17-0267.1>, 2018b.
- 615
- Tilmes, S., Richter, J. H., Kravitz, B., MacMartin, D. G., Glanville, A. S., Vioni, D., et al.: Sensitivity of total column ozone to stratospheric sulfur injection strategies. *Geophysical Research Letters*, 48, e2021GL094058. <https://doi.org/10.1029/2021GL094058>, 2021.
- Tilmes, S., Vioni, D., Jones, A., Haywood, J., Séférian, R., Nabat, P., Boucher, O., Bednarz, E. M., and Niemeier, U.: Stratospheric ozone response to sulfate aerosol and solar dimming climate interventions based on the G6 Geoengineering Model Intercomparison Project (GeoMIP) simulations, *Atmos. Chem. Phys.*, 22, 4557–4579, <https://doi.org/10.5194/acp-22-4557-2022>, 2022.
- 620
- Vioni, D., Pitari, G., Tuccella, P., and Curci, G.: Sulfur deposition changes under sulfate geoengineering conditions: quasi-biennial oscillation effects on the transport and lifetime of stratospheric aerosols, *Atmos. Chem. Phys.*, 18, 2787–2808, <https://doi.org/10.5194/acp-18-2787-2018>, 2018.
- 625
- Vioni, D., MacMartin, D. G., Kravitz, B., Boucher, O., Jones, A., Lurton, T., Martine, M., Mills, M. J., Nabat, P., Niemeier, U., Séférian, R., and Tilmes, S.: Identifying the sources of uncertainty in climate model simulations of solar radiation modification with the G6sulfur and G6solar Geoengineering Model Intercomparison Project (GeoMIP) simulations, *Atmos. Chem. Phys.*, 21, 10039–10063, <https://doi.org/10.5194/acp-21-10039-2021>, 2021
- 630
- Vioni, D., Bednarz, E.M., Lee, W.R., Kravitz, B., Jones, A., Haywood, J.M., MacMartin, D.G., Climate response to off-equatorial stratospheric sulfur injections in three Earth System Models - part 1: experimental protocols and surface changes, in prep, 2022.
- 635
- Weisenstein, D. K., Vioni, D., Franke, H., Niemeier, U., Vattioni, S., Chiodo, G., Peter, T., and Keith, D. W.: An interactive stratospheric aerosol model intercomparison of solar geoengineering by stratospheric injection of SO<sub>2</sub> or accumulation-mode sulfuric acid aerosols, *Atmos. Chem. Phys.*, 22, 2955–2973, <https://doi.org/10.5194/acp-22-2955-2022>, 2022.
- 640

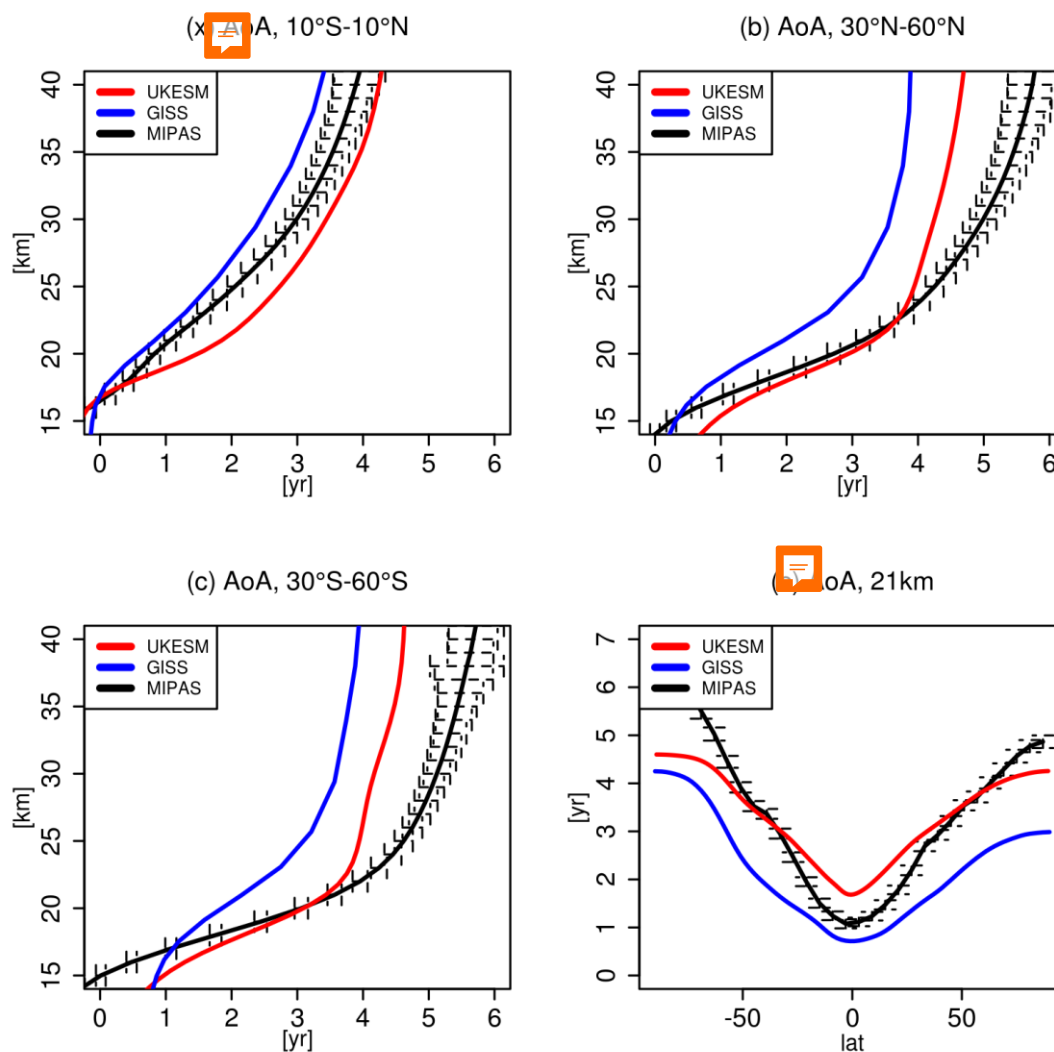


645

**Figure 1.** Yearly mean changes in surface area density [ $10^{-7} \text{ cm}^2/\text{cm}^3$ ], averaged over the last 8 years of the simulations, compared to the same period in the SSP2-4.5 run for CESM (column 1), UKESM (column 2), GISSmodal (column 3) and GISSbulk (column 4). The SAD values were calculated off-line using monthly mean diagnostics, see text for details.

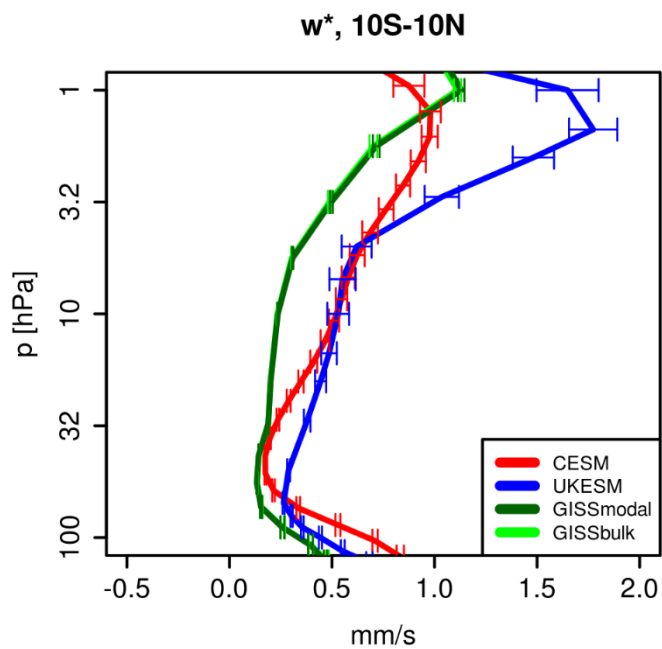


650 **Figure 2.** Climatological mass streamfunction of the residual circulation, averaged over 2035-2064, in the control SSP2-4.5 for each of the four models.

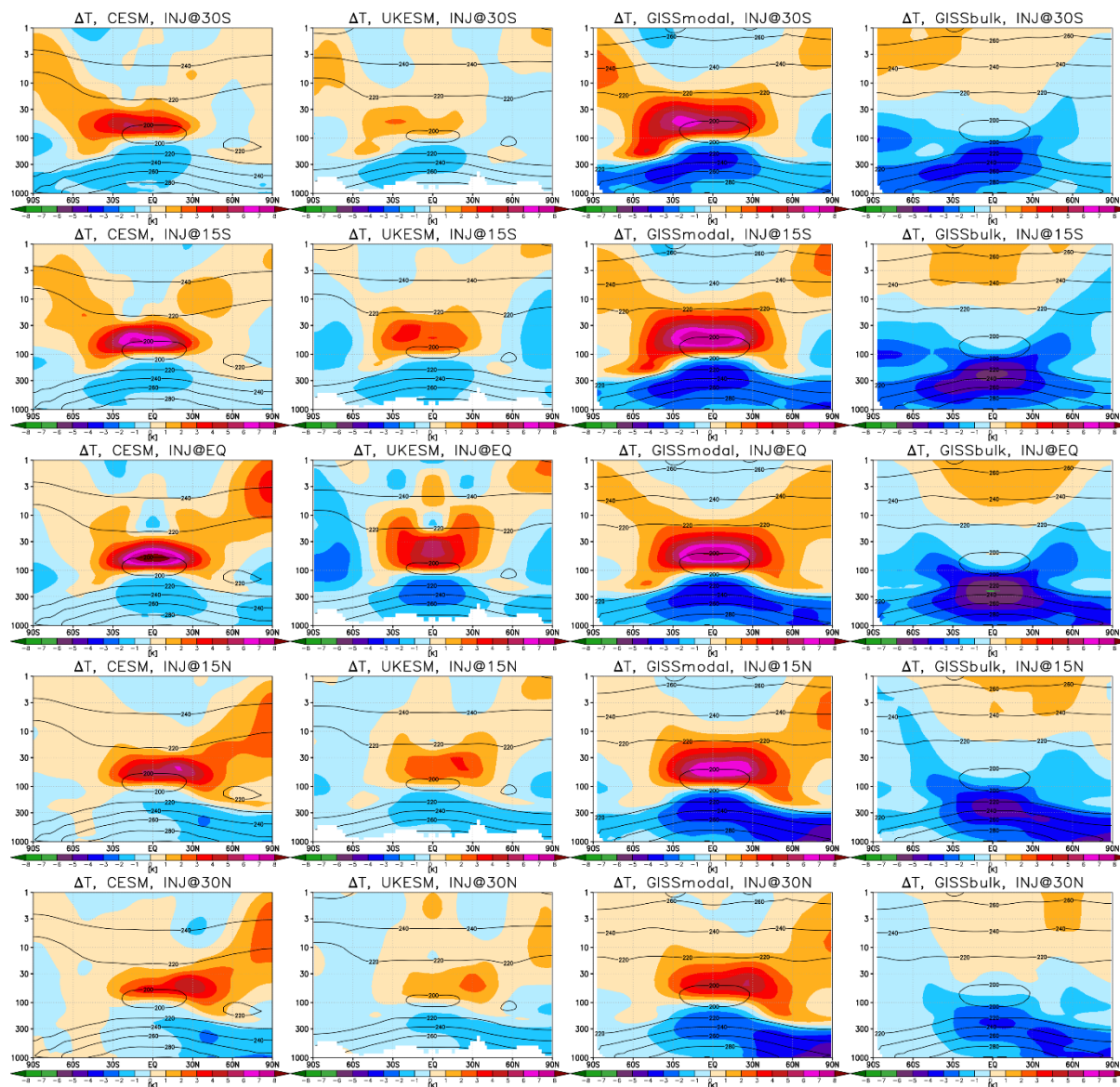


655 **Figure 3.** Normalised age-of-air [yr] for (a) 10°S-10°N, (b) 30°S-60°N, (c) 30°N-60°S and (d) at 21 km, diagnosed from the **UKESM** and GISSbulk CMIP6 historical integration (red). Black lines show the corresponding AoA derived from the MIPAS SF6 satellite observations (black; Stiller et al., 2020). Both model and observed AoA were averaged over the 7-year period from May 2005 to Apr 2012 inclusive. Both model and observed AoA were normalised to be zero at the tropical tropopause by subtracting the values calculated in each case for the tropical tropopause layer (here approximated as mean over 25°S-25°N, 16-17 km). **CESM not** included as no AoA diagnostic is available from its historical CMIP6 simulations.

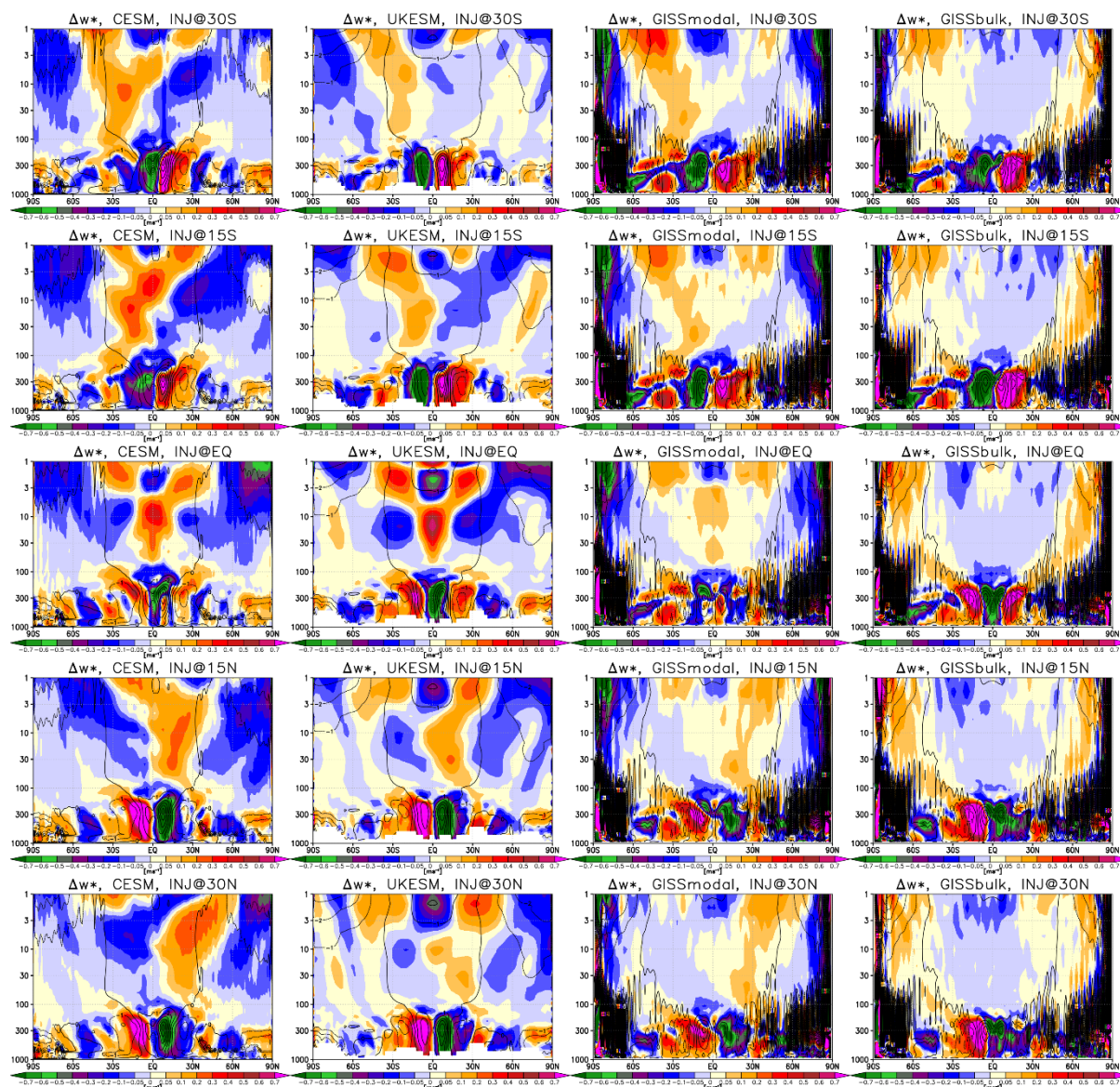
660



665 **Figure 4.** Climatological transformed vertical residual velocity, averaged over 2035-2064 and 10°S-10°N, in the control SSP2-4.5 for each of the four models. Error bars denote  $\pm 2$  standard error of the mean.

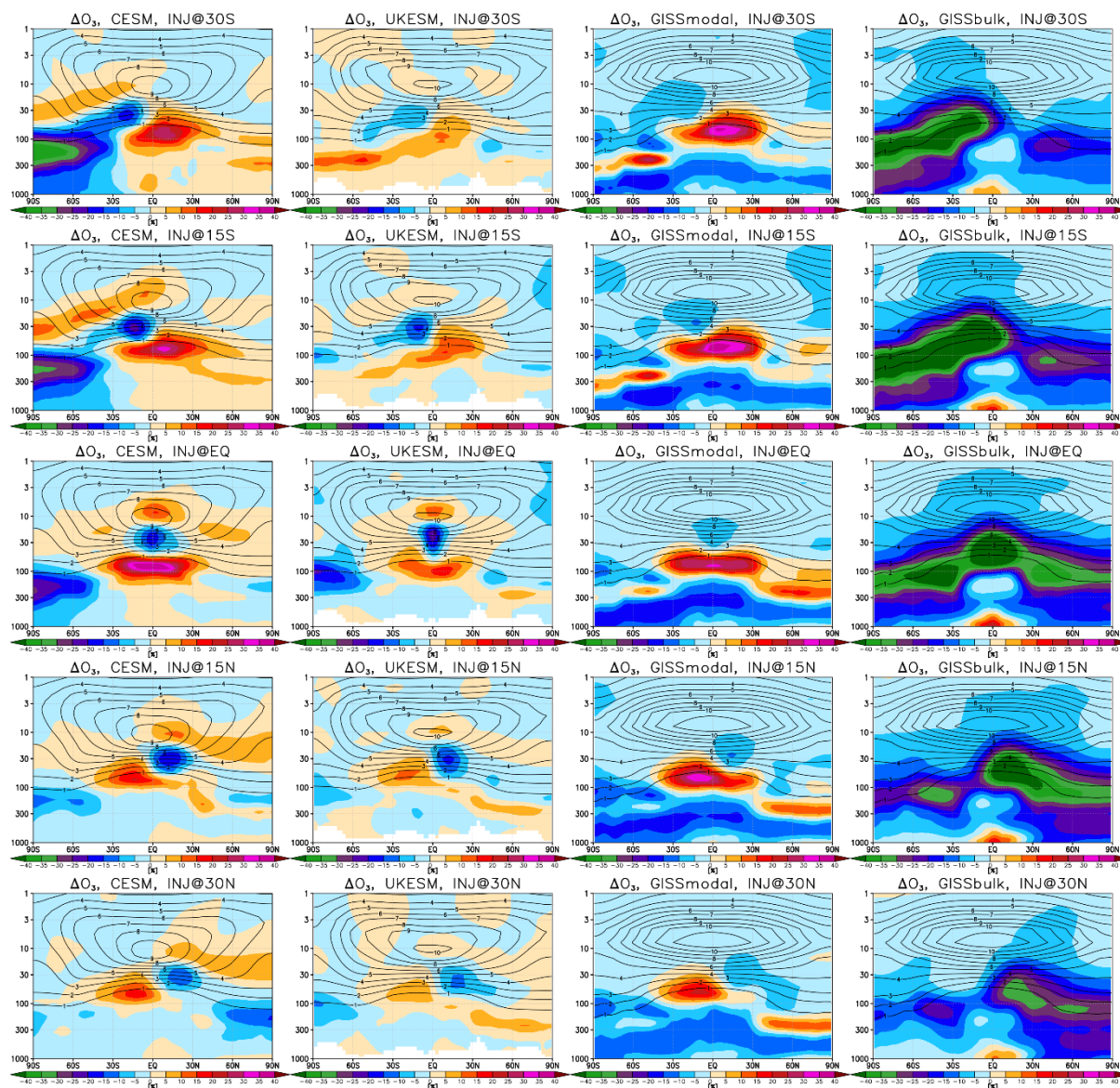


670 **Figure 5.** Shading: yearly mean changes in temperature [K], averaged over the last 8 years of the simulations, compared to the same period in the SSP2-4.5 run for CESM (column 1), UKESM (column 2), GISSmodal (column 3) and GISSbulk (column 4). **Contours** show the values in the control SSP2-4.5 run for reference.

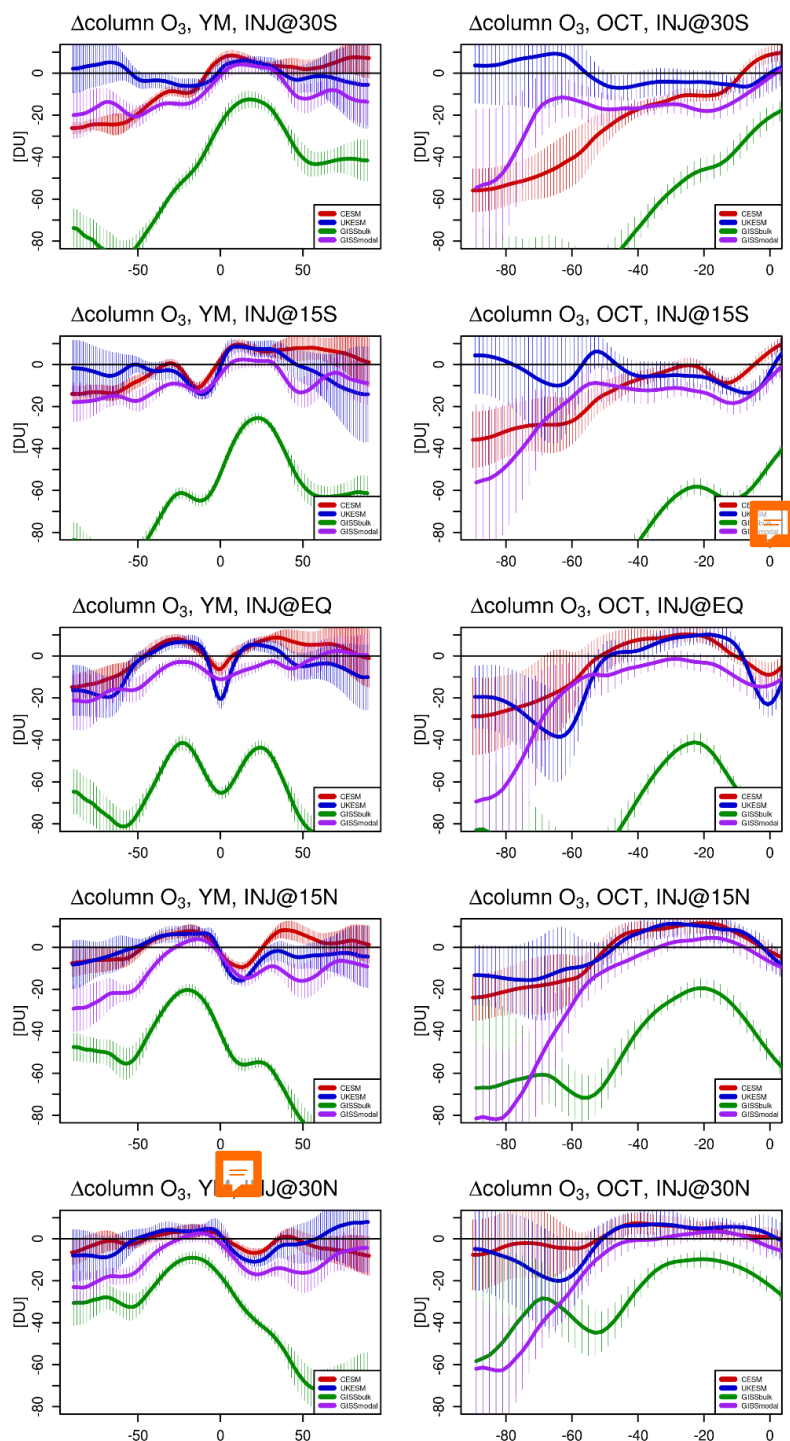


675

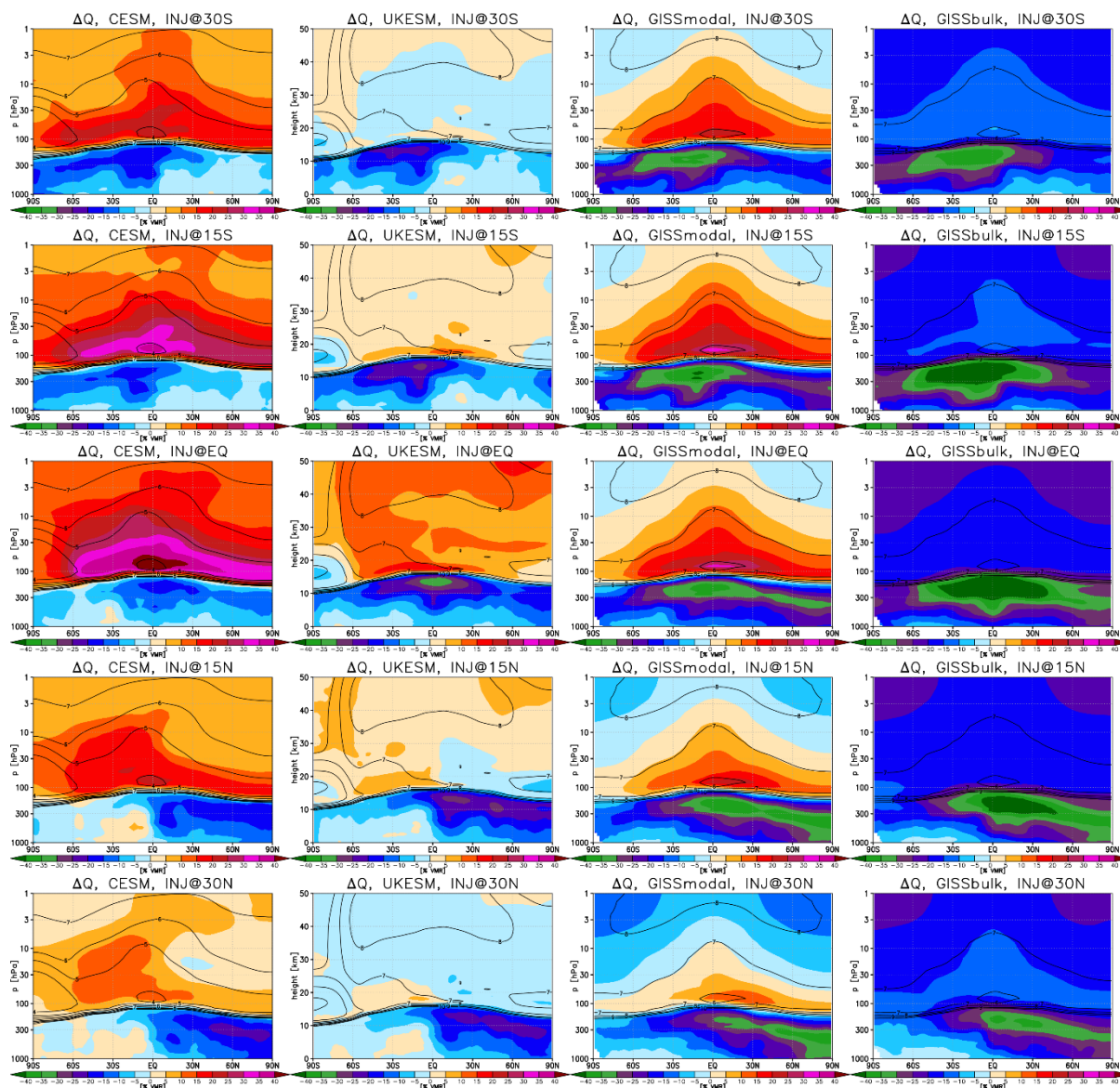
**Figure 6. Shading:** Yearly mean changes in transformed vertical velocity [mm/s], averaged over the last 8 years of the simulations, compared to the same period in the SSP2-4.5 run for CESM (column 1), UKESM (column 2), GISSmodal (column 3) and GISSbulk (column 4). Positive values indicate anomalous upwelling. **Contours** show the vertical velocities in the control SSP2-4.5 run for reference.



680 **Figure 7.** Shading: Yearly mean changes in ozone [%], averaged over the last 8 years of the simulations, compared to the same period in the SSP2-4.5 run for CESM (column 1), UKESM (column 2), GISSmodal (column 3) and GISSbulk (column 4). Contours show the ozone mixing ratios [ppbv] in the control SSP2-4.5 run for reference.



685 **Figure 8.** Yearly (left) and October (right) mean changes in total column ozone [DU], averaged over the last 8 years of the simulations, compared to the same period in the SSP2-4.5 run for **CESM (red), UKESM (blue), GISSmodal (purple) and GISSbulk (green).** Error bars indicate  $\pm 2$  standard errors of the difference in means.



690

**Figure 9.** Yearly mean changes in specific humidity [%], averaged over the last 8 years of the simulations, compared to the same period in the SSP2-4.5 run for CESM (column 1), UKESM (column 2), GISSmodal (column 3) and GISSbulk (column 4). Contours indicate the corresponding values in the SSP2-4.5 experiment in the units of ppmv for reference.

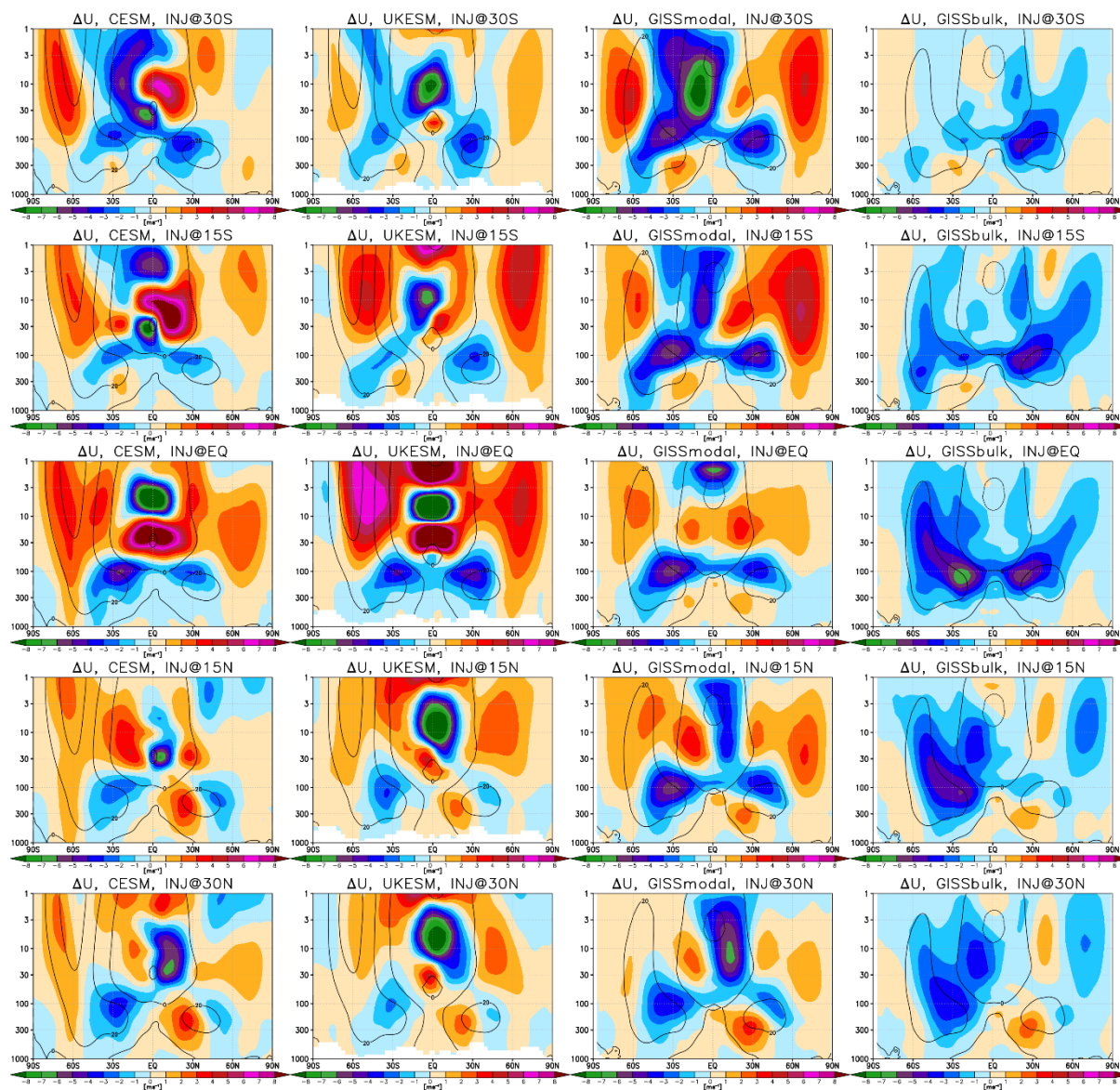


Figure 10. As in Fig. 5 but for zonal wind changes [ $\text{m s}^{-1}$ ].